Aleksej Jochim and Christian Näther*

Formation of di- and polynuclear Mn(II) thiocyanate pyrazole complexes in solution and in the solid state

https://doi.org/10.1515/znb-2018-0104
Received May 23, 2018; accepted July 21, 2018

Abstract: Reaction of $Mn(NCS)_2$ with pyrazole leads to the formation of three compounds with the compositions $Mn(NCS)_2(pyrazole)_4$ (**1**), $[Mn(NCS)_2]_2(pyrazole)_6$ (**2**) and $Mn(NCS)_2(pyrazole)_2$ (**3**). Compound **1**, already reported in the literature, consists of discrete complexes, in which the Mn(II) cations are octahedrally coordinated by four pyrazole ligands and two terminally N-bonded thiocyanate anions. In compound **2** each of the two Mn(II) cations are coordinated octahedrally by three pyrazole ligands and one terminal as well as two bridging thiocyanate anions, which link the metal cations into dimers. In compound **3** also octahedrally coordinated Mn(II) cations are present but they are linked into chains *via* centrosymmetric pairs of μ-1,3-bridging thiocyanate anions. Upon heating compound **1** loses the pyrazole co-ligands stepwise and is transformed into the chain compound **3** *via* the dimer **2** that is formed as an intermediate. Magnetic measurements on compounds **2** and **3** reveal dominating antiferromagnetic interactions, as already observed for 1D $Mn(NCS)_2$ coordination compounds with pyridine based co-ligands.

Keywords: crystal structures; magnetic properties; Mn coordination compounds; pyrazole; thermal properties; thiocyanate ligands.

Dedicated to: Professor Bernt Krebs on the occasion of his 80th birthday.

***Corresponding author: Christian Näther,** Institut für Anorganische Chemie, Christian-Albrechts-Universität zu Kiel, Max-Eyth-Straße 2, 24118 Kiel, Germany, Fax: +49-431-8801520,
E-mail: cnaether@ac.uni-kiel.de
Aleksej Jochim: Institut für Anorganische Chemie, Christian-Albrechts-Universität zu Kiel, Max-Eyth-Straße 2, 24118 Kiel, Germany

1 Introduction

Thiocyanate anions are versatile ligands that can coordinate to metal cations in many different ways. The most prominent coordination is the so-called N- or S-terminal coordination, in which the anionic ligands are only connected *via* the N or the S atom to the metal centers [1–7]. Compared to the N-coordination the latter mode is rare and only found with strong chalcophilic cations like, e.g. Ag(I), Pd(II) or Pt(II) [8–13]. From a structural point of view the bridging modes are much more interesting, because in this case metal cations can be linked into a variety of motifs like, e.g. dimers, chains or layers [14–20]. The large number of coordination modes and the structural diversity of such compounds are expressed by the fact, that an increasing number of different polymorphic or isomeric modifications of thiocyanate compounds were reported recently [21–24]. Moreover, thiocyanate anions can mediate magnetic exchange and in this context many papers reported on new magnetic compounds with several of them showing magnetic ordering upon cooling [25–41]. Our investigations focus on thio- and selenocyanate compounds with 3D metal cations, like, e.g. Mn(II), Fe(II), Co(II), and Ni(II) which are additionally coordinated by N-donor co-ligands. In most cases two different compounds are obtained. Discrete complexes with the general composition $M(NCX)_2(L)_4$ (X=S, Se and L = co-ligand) with octahedral coordination of the metal cations and terminally N-bonded anionic ligands as well as compounds with the composition $M(NCX)_2(L)_2$, in which the octahedrally coordinated metal cations are linked by μ-1,3-bridging anionic ligands into chains or layers [42–48]. In solution the discrete complexes are usually more stable, which means that the bridging compounds are sometimes difficult to prepare. However, if the complexes are heated the co-ligands can be removed in a discrete step, which leads to the formation of the bridging compounds in quantitative yield. In some cases metastable compounds like, e.g. polymorphs or isomers are obtained that are different from those obtained from solution. It is noted, that the synthesis of coordination compounds by typical solid state synthesis is not uncommon and several

approaches have already been reported [49–52]. However, in most cases 1D compounds are obtained, in which the metal cations are linked by pairs of anionic ligands into chains. Dependent on the nature of the metal cation the magnetic exchange along the chain is usually different. For, e.g. Ni(II) and Co(II) it is ferromagnetic, whereas for compounds based on $Mn(NCS)_2$ it is usually antiferromagnetic [32–34, 53–55]. For the latter usually simple paramagnetic behavior is observed, but some of them show antiferromagnetic ordering upon cooling [53–55].

However, what is common to all of the compounds is the fact, that they always contain pyridine derivatives as co-ligands, which are usually substituted in 4-position. Most of these ligands are relatively volatile and this might be the reason, why they can easily be removed by thermal treatment, leading to the formation of the bridged compounds. Therefore, the question arises if similar compounds can be prepared with other co-ligands and how this will influence the thermal behavior and the magnetic properties. In the beginning we selected pyrazole as a ligand, for which already some discrete complexes with the composition $M(NCS)_2(pyrazole)_4$ have been reported with M=Mn [56], Co [57], and Ni [57, 58]. Compounds with bridging anionic ligands and these cations are unknown but there is one 1D Cd compound with the composition $[Cd(NCS)_2(pyrazole)_2]_n$, which indicates that more of such coordination polymers might be available [59].

2 Results and discussion

2.1 Synthesis

The reaction of $Mn(NCS)_2$ with pyrazole in different molar ratios yielded three different crystalline phases, of which one could be identified by X-ray powder diffraction (XRPD) as $Mn(NCS)_2(pyrazole)_4$ (**1**) reported recently. For the other two phases elemental analyses suggested a composition of $[Mn(NCS)_2]_2(pyrazole)_6$ (**2**) and $Mn(NCS)_2(pyrazole)_2$ (**3**). An IR spectroscopic measurement on compound **2** has shown that two bands for the CN stretching vibration of the thiocyanate anions are observed at 2068 and at 2097 cm^{-1}. The first value is very similar to that observed in **1** (2064 cm^{-1}), indicating that terminally bound anionic ligands are present in **2**. The second value is strongly shifted to higher values and in the range for those, typically observed for bridging anionic ligands. Therefore, it is highly likely that compound **2** consists of dimers with terminal and bridging thiocyanate anions. For compound **3** the CN stretch is surprisingly observed at 2072 cm^{-1} which is at the borderline values usually observed for terminal and bridging thiocyanate anions and in this case no predictions can be made. However, for compounds **2** and **3** crystals suitable for single crystal X-ray diffraction analysis could be prepared and structurally characterized.

2.2 Crystal structures

2.2.1 Crystal structure of $[Mn(NCS)_2]_2(pyrazole)_6$ (2)

Compound **2** crystallizes in the monoclinic space group $P2_1/n$ with the asymmetric unit consisting of one Mn(II) cation, two thiocyanate anions and three pyrazole molecules in general positions. Each of the Mn(II) cations is octahedrally coordinated by three pyrazole molecules as well as one terminal and two μ-1,3-bridging thiocyanate anions thus producing a dinuclear complex, as already indicated by the IR spectroscopic measurements (Fig. 1).

The Mn–N distance to the terminal thiocyanate anion of 2.162(2) Å is slightly shorter than that to the bridging anionic ligand of 2.1854(2) Å, which might be traced back to steric repulsion (Table 1). The Mn–N distances to the pyrazole ligands between 2.232(2) and 2.257(2) Å are significantly longer than that to the thiocyanate anions (Table 2).

The bond angles, which range from 84.99(5) to 95.11(5)° and from 174.77(5)° to 177.35(8)°, indicate a slight distortion of the coordination polyhedron. This can be quantified using the values of the octahedral angle variance $\sigma_{\theta<oct>}{}^2$ and the mean octahedral quadratic elongation λ_{oct} introduced by Robinson et al. [60]. Comparing the corresponding values for compound **2** ($\sigma_{\theta<oct>}{}^2 = 7.21$, $\lambda_{oct} = 1.01$)

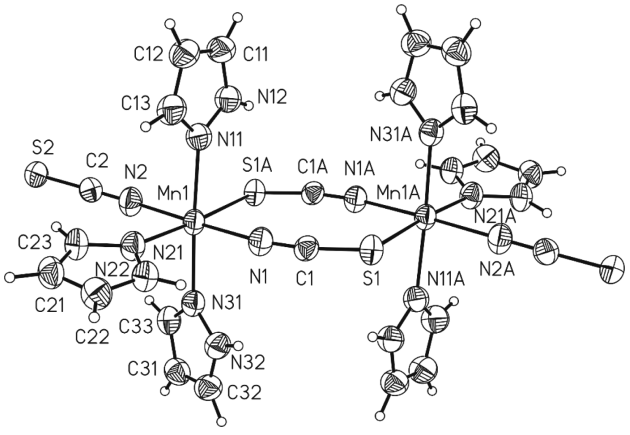

Fig. 1: View of the dinuclear complex **2** with labeling and displacement ellipsoids drawn at the 50% probability level. Symmetry codes: A: $-x+1$, $-y+1$, $-z+1$.

Table 1: Selected bond lengths and angles (Å, deg) for compound **2**.

Mn(1)–N(1)	2.1854(18)	Mn(1)–N(21)	2.2315(18)
Mn(1)–N(2)	2.1621(19)	Mn(1)–N(31)	2.2566(19)
Mn(1)–N(11)	2.2466(19)	Mn(1)–S(1A)	2.7514(7)
N(2)–Mn(1)–N(1)	177.35(8)	N(21)–Mn(1)–N(31)	90.86(7)
N(2)–Mn(1)–N(21)	89.80(7)	S(1)–Mn(1A)	2.7514(6)
N(1)–Mn(1)–N(21)	90.11(7)	N(11)–Mn(1)–N(31)	176.57(6)
N(2)–Mn(1)–N(11)	90.51(8)	N(2)–Mn(1)–S(1A)	84.99(5)
N(1)–Mn(1)–N(11)	92.14(7)	N(1)–Mn(1)–S(1A)	95.11(5)
N(21)–Mn(1)–N(11)	92.54(7)	N(21)–Mn(1)–S(1A)	174.77(5)
N(2)–Mn(1)–N(31)	90.00(7)	N(11)–Mn(1)–S(1A)	87.03(5)
N(1)–Mn(1)–N(31)	87.35(7)	N(31)–Mn(1)–S(1A)	89.64(5)

Symmetry code for the generation of equivalent atoms: A: $-x+1$, $-y+1$, $-z+1$.

Table 2: Hydrogen bonding (Å, deg) for compound **2**.

	D···A	H···A	<(D–H···A)
N(12)–H(12)···S(1A)	3.335(2)	2.73	127.5
N(12)–H(12)···S(2B)	3.622(2)	2.87	144.2
N(22)–H(22A)···S(2D)	3.320(2)	2.61	138.1
N(32)–H(32A)···S(2E)	3.321(2)	2.51	153.4

Symmetry codes: A: $-x+1$, $-y+1$, $-z+1$; B: $-x+1/2$, $y+1/2$, $-z+3/2$; D: $-x+3/2$, $y+1/2$, $-z+3/2$; E: $x+1/2$, $-y+1/2$, $z-1/2$.

with those for compound **1** ($\sigma_{\theta,oct}^2 = 3.05$, $\lambda_{oct} = 1.00$) shows that the coordination octahedron of the dimer **2** is more distorted than that of the discrete octahedral complex **1**. This is expected as the Mn(II) cation of compound **2** is coordinated by nitrogen as well as sulfur while in compound **1** the metal cation is coordinated solely by nitrogen atoms.

The dimeric units are interconnected *via* hydrogen bonding between the pyrazole N–H groups and the thiocyanate sulfur atoms forming a three dimensional network (Fig. 2, Table 2).

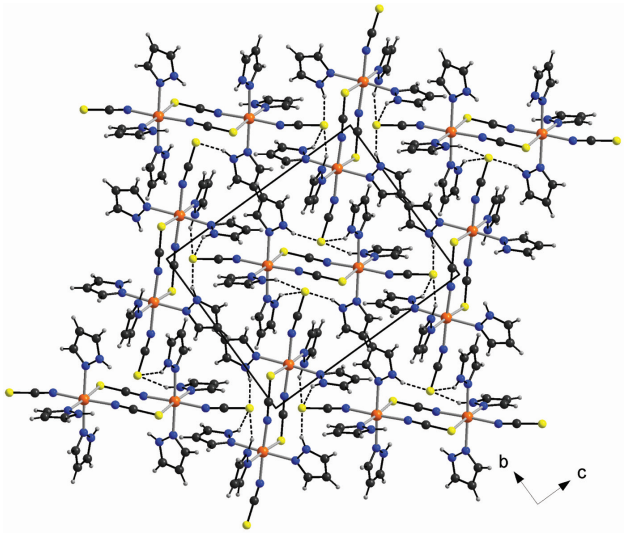

Fig. 2: Crystal structure of **2** with view along the crystallographic *a* axis with intermolecular hydrogen bonding shown as dashed lines.

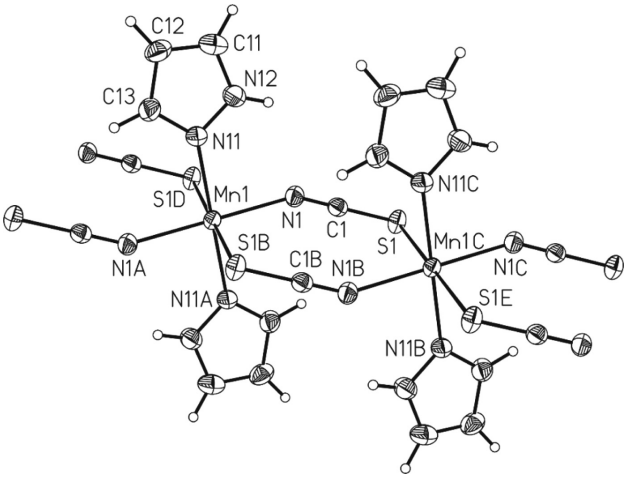

Fig. 3: View of a part of a chain in crystals of **3** with labeling and displacement ellipsoids drawn at the 50% probability level. Symmetry codes: A: $-x+1$, $-y+1$, $-z+1$; B: $-x$, $-y+1$, $-z+1$; C: $x-1$, y, z; D: $x+1$, y, z; E: $-x-1$, $-y+1$, $-z+1$.

2.2.2 Crystal structure of $Mn(NCS)_2(pyrazole)_2$ (3)

Compound **3** crystallizes in the monoclinic space group $P2_1/c$ with the asymmetric unit containing one thiocyanate anion and one pyrazole molecule in general positions as well as one Mn(II) cation that occupies a center of inversion. The Mn(II) cations are connected *via* centrosymmetric pairs of thiocyanate anions into chains. Two pyrazole molecules occupy the axial positions, whereas the two S and two thiocyanate N atoms are located in the basal plane in *trans*-position leading to a slightly distorted octahedral coordination environment (Fig. 3).

As in compound **2**, the Mn–N distances to the anionic ligands are shorter than those to the pyrazole co-ligands (Table 3). However, the thiocyanate Mn–N distances are comparable to those in **2**, whereas the Mn–S distance is significantly shorter than in the dimer **2**, which points to a stronger interaction (compare Tables 1 and 3). The Mn–N distances to the pyrazole ligands are comparable to those found in compound **2**. It is noted that the C–N distance of the thiocyanate anion is as long as that in the terminally N-bonded anion in the dimer **2** and significantly shorter than that of the bridging anionic ligand. This might be the reason why the C–N stretch is shifted to much lower

Table 3: Selected bond lengths and angles (Å, deg) for compound **3**.

Mn(1)–N(1)	2.1660(13)	Mn(1)–N(11A)	2.2353(13)
Mn(1)–N(1A)	2.1660(13)	Mn(1)–S(1B)	2.6850(4)
Mn(1)–N(11)	2.2353(13)	Mn(1)–S(1C)	2.6850(4)
N(1)–Mn(1)–N(1A)	180.00(7)	N(11)–Mn(1)–S(1B)	87.60(4)
N(1)–Mn(1)–N(11)	88.63(5)	N(11A)–Mn(1)–S(1B)	92.40(4)
N(1A)–Mn(1)–N(11)	91.37(5)	N(1)–Mn(1)–S(1C)	93.53(4)
N(1)–Mn(1)–N(11A)	91.37(5)	N(1A)–Mn(1)–S(1C)	86.47(4)
N(1A)–Mn(1)–N(11A)	88.63(5)	N(11)–Mn(1)–S(1C)	92.40(4)
N(11)–Mn(1)–N(11A)	180.0	N(11A)–Mn(1)–S(1C)	87.60(4)
N(1)–Mn(1)–S(1B)	86.47(4)	S(1B)–Mn(1)–S(1C)	180.0
N(1A)–Mn(1)–S(1B)	93.53(4)		

Symmetry codes for the generation of equivalent atoms: A: $-x+1$, $-y+1$, $-z+1$; B: $x+1$, y, z; C: $-x$, $-y+1$, $-z+1$.

values than expected. As in compound **2**, the octahedra are slightly distorted and the octahedral angle variance and mean octahedral quadratic elongation values ($\sigma_{\theta,oct}{}^2 = 7.30$, $\lambda_{oct} = 1.02$) indicate that the distortion of the coordination environment is comparable to that in compound **2**.

As mentioned above, the Mn(II) cations are linked into chains by pairs of anionic ligands but the topology of the chains is significantly different from that of the corresponding 1D compounds with pyridine derivatives as co-ligands. In these compounds the metal cations and the thiocyanate anions are always co-planar, but in compound **3**, the MnN_2S_2 planes of neighboring cations are shifted relative to each other, leading to the formation of corrugated chains (Fig. 4: top). However, for the chain compounds with pyridine derivatives only two different arrangements of the chains are observed. In one group the N–N vectors of the pyridine N atoms are parallel, whereas in the second group they are canted. In the crystal structure of compound **3**, the latter motif is observed (Fig. 4: bottom).

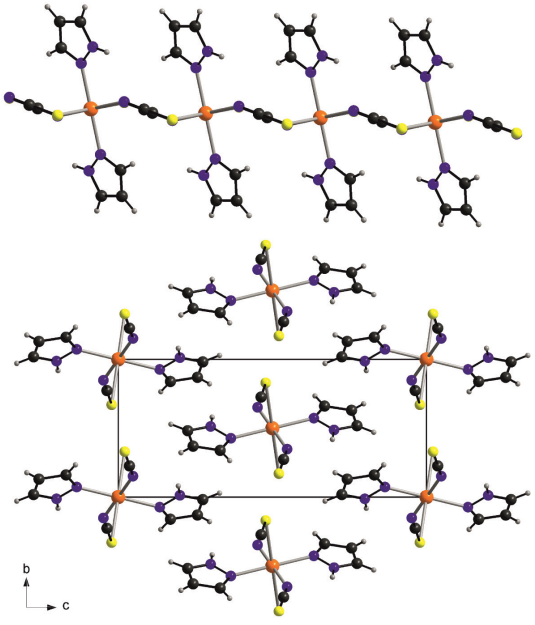

Fig. 4: Crystal structure of **3** with view of a single chain (top) and along the crystallographic *b* axis (bottom).

The single crystal data were used to calculate the corresponding XRPD patterns, and the results were compared with the experimental pattern showing clearly that compounds **1**, **2** and **3** were obtained as pure phases. For compound **3**, small differences in the peak positions were found, which can be traced back to the fact that the single crystal data collection was performed at 170 K. Therefore, the lattice parameters were additionally determined by a Pawley fit using the XRPD data measured at room-temperature and in this case perfect agreement is observed (Fig. 5).

2.3 Thermoanalytical investigations

To check if compound **1** can be transformed into the chain compound **3** as usually observed in such compounds, measurements using simultaneous differential thermoanalysis and thermogravimetry (DTA-TG) were performed (Fig. 6). Upon heating three poorly resolved mass steps are observed, already indicated by the DTG curve, which are accompanied with endothermic events in the DTA curve (Fig. 6). The experimental mass loss in the first and second step of 15.3 and 15.4%, respectively, is in good agreement with that calculated for the loss of one pyrazole molecule in each step (Δm_{calcd} – 1 pyrazole = 15.4%). In the third TG step, the remaining two pyrazole ligands are lost leading to the formation of $Mn(NCS)_2$ which decomposes upon further heating. The DTG curve shows that the third step consists of two different processes that cannot be fully resolved. However, the fact that only one co-ligand is removed in the first step indicates that a compound with the composition $Mn(NCS)_2(pyrazole)_3$ is formed, that might correspond to the dimer **2**.

To identify the intermediates of the thermal degradation of compound **1** the residues formed after the first and second TG step were isolated and analyzed by XRPD (Fig. 7). The powder diffraction pattern after the first step is identical with that calculated for compound **2** and that after the second step corresponds to the chain compound **3**. This is surprising, because usually such discrete complexes loose two co-ligands simultaneously and are transformed directly into chain or layer compounds, without the formation of dinuclear complexes, even if the latter are available from solution.

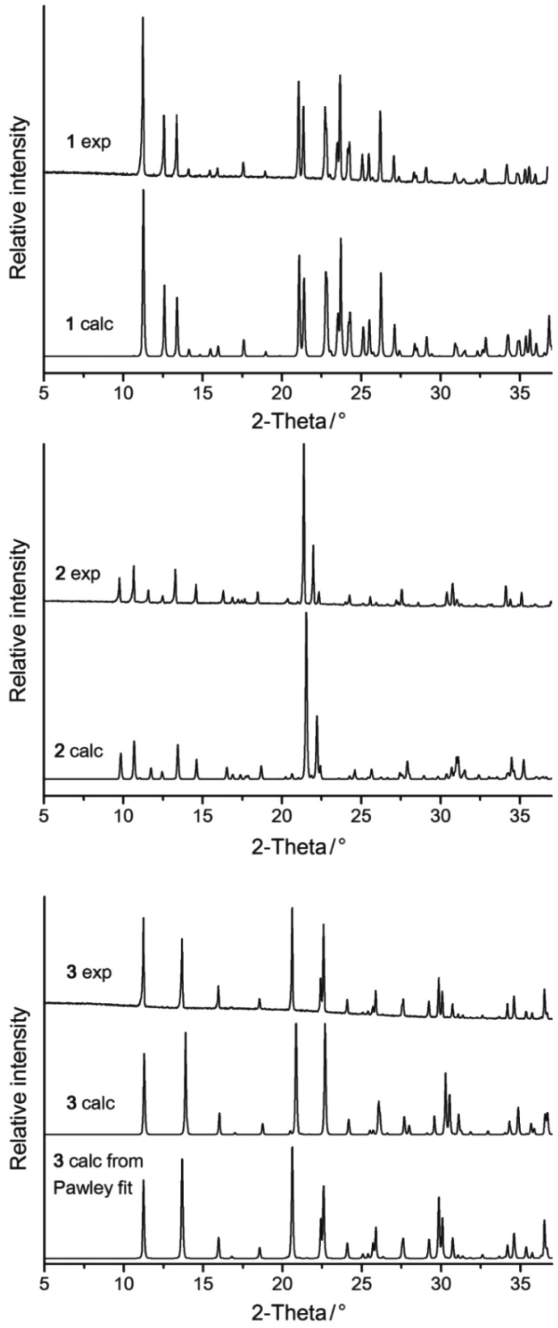

Fig. 5: Experimental and calculated XRPD patterns for compounds **1**, **2** and **3**, the calculations being based on the single crystal data. For compound **3**, the lattice parameters obtained from a Pawley fit of the powder pattern measured at room temperature were also employed.

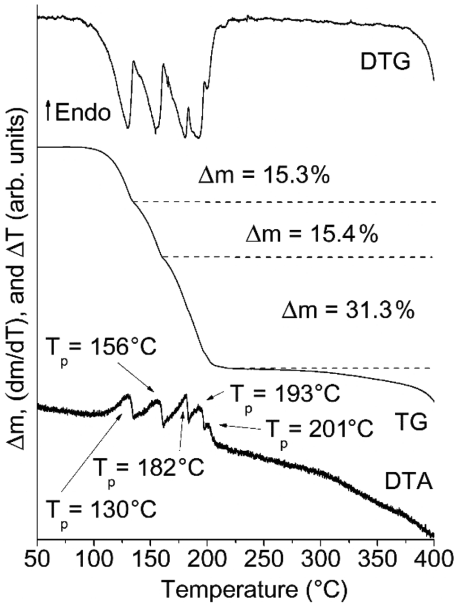

Fig. 6: DTA, TG and DTG curves for **1** at a heating rate of 1°C min^{-1}.

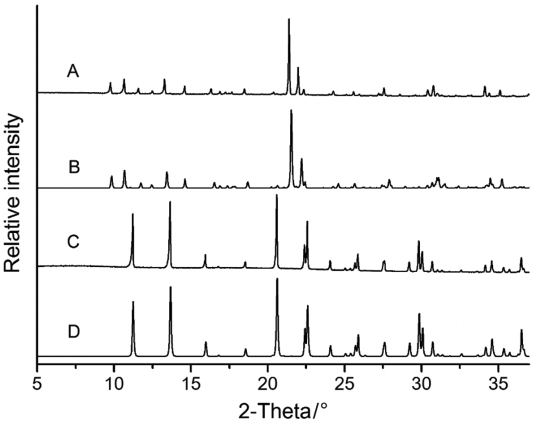

Fig. 7: Experimental XRPD patterns of the residues obtained after the first (A) and second (C) step in the TG measurement of compound **1**, together with the pattern calculated for compounds **2** (B) and **3** (D). For compound **3** the pattern calculated from the lattice parameters determined by a Pawley fit is shown.

2.4 Magnetic measurements

The magnetic properties of compounds **2** and **3** were investigated by susceptibility measurements in the temperature range from 300 to 2 K applying a magnetic field of $H_{DC} = 0.1$ T. Upon cooling the product χT first does not change significantly, but below 100 K it starts do decrease rapidly (Fig. 8). This behavior indicates dominating antiferromagnetic interactions between the Mn(II) cations that are connected by the thiocyanate anions. This is also shown by the values of the Weiss constant derived from a Curie-Weiss fit leading to values of $\theta = -11.8$ K for compound **2** and $\theta = -27.1$ K for compound **3.**

The effective magnetic moment μ_{eff} of compound **2** at room temperature amounts to $\mu_{eff} = 5.92\ \mu_B$, which is

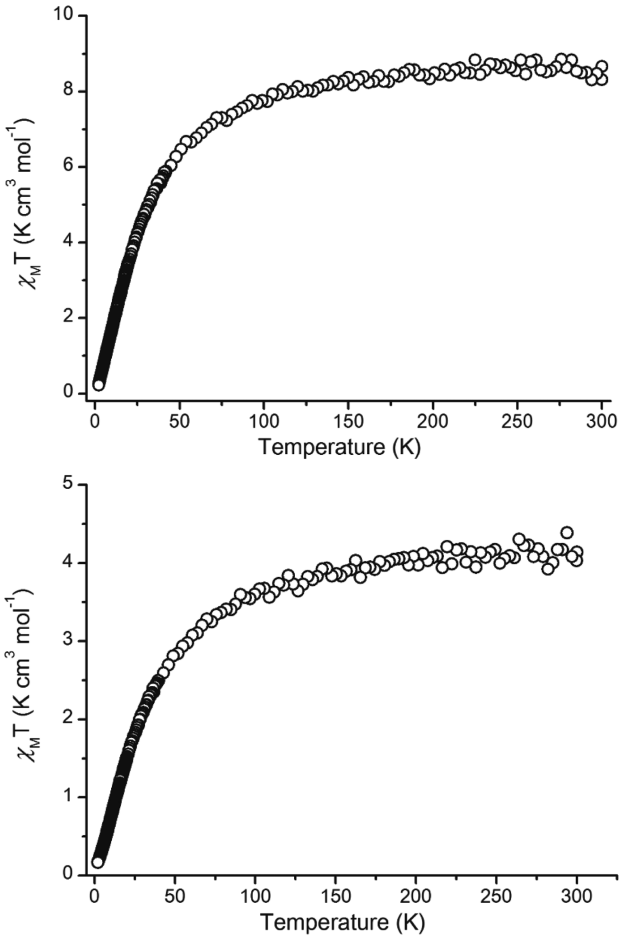

Fig. 8: Temperature dependence of the χT product for **2** (top) and **3** (bottom) at $H_{DC} = 0.1$ T.

in perfect agreement with the spin only value for a high-spin Mn(II) cation in an octahedral coordination ($S = 5/2$, $g = 2.00$). For compound **3** ($\mu_{eff} = 6.03\ \mu_B$) the experimental value deviates slightly, which might indicate the presence of a minor impurity that cannot be detected by XRPD. This is in agreement with the χ vs. T curve for **3**, that shows a maximum which is indicative of antiferromagnetic ordering, but on further cooling the susceptibility increases again, pointing to a paramagnetic impurity. This has also been observed for other $Mn(NCS)_2$ compounds with pyridine derivatives as co-ligands [55]. As mentioned above, the majority of the 1D $Mn(NCS)_2$ compounds reported in the literature show dominating antiferromagnetic exchange interactions, which indicates that the co-ligand has only a minor influence on the overall magnetic behavior. This is in agreement with investigations on compounds not containing pyridine derivatives, which also show predominately antiferromagnetic exchange interactions [30, 61, 62].

3 Conclusions

In the present contribution, new compounds with the compositions $[Mn(NCS)_2]_2(pyrazole)_6$ (**2**) and $Mn(NCS)_2(pyrazole)_2$ (**3**) have been prepared from reactions carried out in isolution. Both compounds can also be obtained by thermal decomposition of the known compound $Mn(NCS)_2(pyrazole)_4$ (**1**) which upon heating is transformed into **3** *via* **2** as an intermediate. The crystal structure of $[Mn(NCS)_2]_2(pyrazole)_6$ consists of dinuclear compounds in which the two Mn(II) cations are connected by a pair of thiocyanate anions, while compound **3** forms chains in which the metal cations are also connected by pairs of anionic ligands. Therefore, the structure of **1** is strongly correlated to that of **2** and **3** and can formally be transformed into these degradation products by stepwise replacement of the N atoms of the co-ligand in **1** by the thiocyanate S atoms that had not been involved in metal coordination. It is noted that a few of such dinuclear complexes have already been described in the literature, but usually they do not occur as intermediates upon heating of the corresponding mononuclear complexes, which might be traced back to the influence of the kinetics of such solid state reactions. Magnetic investigations on compounds **2** and **3** have revealed dominating antiferromagnetic exchange interactions, which are also observed in similar compounds containing pyridine derivatives and other co-ligands. Thus the nature of the co-ligand do not have a strong influence on the magnetic behavior of such $Mn(NCS)_2$ coordination compounds.

4 Experimental section

4.1 Synthesis

4.1.1 General

$Ba(NCS)_2 \cdot 3H_2O$ and pyrazole were obtained from Alfa Aesar and used without further purification. $Mn(NCS)_2$ was prepared by the reaction of equimolar amounts of $MnSO_4 \cdot H_2O$ and $Ba(NCS)_2 \cdot 3H_2O$ in water. The resulting white precipitate of $BaSO_4$ was filtered off and the filtrate was concentrated to complete dryness resulting in a yellow residue of $Mn(NCS)_2$.

4.1.2 Syntheses of $Mn(NCS)_2(pyrazole)_4$ (1)

$Mn(NCS)_2$ (171.2 mg, 1.00 mmol) and pyrazole (409.2 mg, 6.0 mmol) were stirred in 0.5 mL ethanol for 1 day. The

colorless residue was filtered off and dried in air. – Elemental analysis for $C_{14}H_{16}MnN_{10}S_2$ (443.4180 g mol^{-1}): C 37.92, H 3.64, N 31.59, S 14.46; found C 37.72, H 3.61, N 31.67, S 14.24.

4.1.3 Syntheses of $[Mn(NCS)_2]_2(pyrazole)_6$ (2)

The reaction of $Mn(NCS)_2$ (171.2 mg, 1.00 mmol) and pyrazole (153.5 mg, 2.25 mmol) in 0.6 mL H_2O yielded a colorless powder after 1 day of stirring. It was filtered off and dried in air. Single crystals of the compound were obtained by dissolution of $Mn(NCS)_2$ (85.6 mg, 0.50 mmol) and pyrazole (68.2 mg, 1.00 mmol) in 0.5 mL ethanol and slow evaporation of the solvent. – Elemental analysis for $C_{22}H_{24}MnN_{16}S_4$ (750.6798 g mol^{-1}): C 35.20, H 3.22, N 29.85, S 17.09; found C 35.35, H 3.26, N 29.94, S 17.27.

4.1.4 Synthesis of $Mn(NCS)_2(pyrazole)_2$ (3)

Suitable single crystals for X-ray structure determination were obtained by the reaction of $Mn(NCS)_2$ (68.2 mg, 0.50 mmol) with pyrazole (34.1 mg, 0.50 mmol) in 0.5 mL ethanol. Slow evaporation of the solvent yielded light yellow crystals. A powder was obtained through stirring of $Mn(NCS)_2$ (171.2 mg, 1.00 mmol) and pyrazole (45.5 mg, 0.67 mmol) in 0.3 mL *n*-butanol for 3 days. – Elemental analysis for $C_8H_8MnN_6S_2$ (307.2617 g mol^{-1}): C 31.27, H 2.62, N 27.36, S 20.87; found C 31.29, H 2.65, N 27.11, S 21.03.

4.2 Methods

CHNS analysis was performed using an EURO EA elemental analyzer, fabricated by EURO VECTOR Instruments.

DTA-TG measurements were performed in a dynamic nitrogen atmosphere in Al_2O_3 crucibles using a STA-PT1600 thermobalance from Linseis. The instrument was calibrated using standard references materials. All measurements were performed with a flow rate of 75 mL min^{-1} and were corrected for buoyancy.

IR spectra were recorded at room temperature on a Bruker Vertex70 FT-IR spectrometer using a broadband spectral range extension VERTEX FM for full mid and far IR.

Magnetic measurements: All magnetic measurements were performed using a PPMS (Physical Property Measurement System) from Quantum Design, which was equipped with a 9 Tesla magnet. The data were corrected for core diamagnetism.

4.3 X-ray powder diffraction (XRPD)

The measurements were performed using a Stoe Transmission Powder Diffraction System (STADI P) with CuKα1 radiation (λ = 1.540598 Å) equipped with a MYTHEN 1 K detector from Dectris and a Ge(111) monochromator from STOE & Cie.

4.4 Single-crystal structure analyses

Data collections were performed with an imaging plate diffraction system IPDS-2 from STOE & Cie using MoKα radiation. Structure solution was performed with SHELXS-97 [63] and structure refinement was performed against F^2 using SHELXL-2014 [64]. A numerical absorption correction was applied using the programs X-RED and X-SHAPE of the program package X-AREA [65–67]. All non-hydrogen atoms were refined with anisotropic displacement parameters. The hydrogen atoms were positioned in idealized geometry and were refined isotropically with $U_{iso}(H) = -1.2\ U_{eq}(C)$ using a riding model. Selected crystal data and details of the structure refinements can be found in Table 4.

Table 4: Selected crystal data and details of the structure determinations for **2** and **3**.

	2	**3**
Formula	$C_{22}H_{24}N_{16}S_4Mn_2$	$C_8H_8N_6S_2Mn$
MW, g mol^{-1}	750.68	307.26
Crystal system	Monoclinic	Monoclinic
Space group	$P2_1/n$	$P2_1/c$
a, Å	9.9294(4)	5.5528(3)
b, Å	11.5780(6)	6.9757(3)
c, Å	14.2236(6)	15.7409(9)
β, deg	92.048(3)	95.364(4)
V, Å^3	1634.14(13)	607.05(5)
T, K	170(2)	170(2)
Z	2	2
D_{calcd}, g cm^{-3}	1.53	1.68
μ, mm^{-1}	1.1	1.4
θ_{max}, deg	27.004	25.991
Refl. collected	23075	8386
Refl. unique	3569	1190
R_{int}	0.1035	0.0257
Min./max. transm.	0.702/0.937	0.587/0.716
Refl. [$F_0 > 4\ \sigma(F_0)$]	3147	1113
Parameters	200	79
R_1 [$F_0 > 4\ \sigma(F_0)$]	0.0392	0.0233
wR_2	0.1079	0.0629
GOF	1.074	1.106
$\Delta\rho_{max/min}$, *e* Å^{-3}	0.36/–0.41	0.28/–0.26

CCDC 1844920 (**2**) and 1844921 (**3**) contain the supplementary crystallographic data for this paper. These data can be obtained free of charge from The Cambridge Crystallographic Data Centre *via* www.ccdc.cam.ac.uk/data_request/cif.

Acknowledgements: We thank Prof. Dr. Wolfgang Bensch for access to his experimental facilities.

References

[1] F. A. Mautner, R. C. Fischer, L. G. Rashmawi, F. R. Louka, S. S. Massoud, *Polyhedron* **2017**, *124*, 237.
[2] F. A. Mautner, M. Scherzer, C. Berger, R. C. Fischer, R. Vicente, S. S. Massoud, *Polyhedron* **2015**, *85*, 20.
[3] R. Uhrecký, I. Ondrejkovičová, D. Lacková, Z. Fáberová, J. Mroziński, B. Kalińska, Z. Padělková, M. Koman, *Inorg. Chim. Acta* **2014**, *414*, 33.
[4] Y. P. Prananto, A. Urbatsch, B. Moubaraki, K. S. Murray, D. R. Turner, G. B. Deacon, R. Batten Stuart, *Aust. J. Chem.* **2017**, *70*, 516.
[5] J. G. Małecki, T. Groń, H. Duda, *Polyhedron* **2012**, *36*, 56.
[6] S. Suckert, L. Germann, R. Dinnebier, J. Werner, C. Näther, *Crystals* **2016**, *6*, 38.
[7] S. S. Massoud, M. Dubin, A. E. Guilbeau, M. Spell, R. Vicente, P. Wilfling, R. C. Fischer, F. A. Mautner, *Polyhedron* **2014**, *78*, 135.
[8] G. A. Bowmaker, C. Pakawatchai, S. Saithong, B. W. Skelton, A. H. White, *Dalton Trans.* **2009**, 2588.
[9] E. Lee, J. Seo, S. S. Lee, K.-M. Park, *Cryst. Growth Des.* **2012**, *12*, 3834.
[10] A. V. Godoy Netto, R. C. G. Frem, A. E. Mauro, E. T. de Almeida, A. M. Santana, J. de Souza, R. H. A. Santos, *Inorg. Chim. Acta* **2003**, *350*, 252.
[11] K. Ha, *Acta Crystallogr.* **2012**, *E68*, m144.
[12] S. Kishi, M. Kato, *Inorg. Chem.* **2003**, *42*, 8728.
[13] K. Ha, *Z. Kristallogr. – New Cryst. Struct.* **2013**, *228*, 313.
[14] F. A. Mautner, C. Berger, R. C. Fischer, S. S. Massoud, *Inorg. Chim. Acta* **2016**, *448*, 34.
[15] M. Maiti, S. Thakurta, D. Sadhukhan, G. Pilet, G. M. Rosair, A. Nonat, L. J. Charbonnière, S. Mitra, *Polyhedron* **2013**, *65*, 6.
[16] S. Das, K. Bhar, S. Chattopadhyay, P. Mitra, V. J. Smith, L. J. Barbour, B. K. Ghosh, *Polyhedron* **2012**, *38*, 26.
[17] S. Suckert, M. Rams, M. M. Rams, C. Näther, *Inorg. Chem.* **2017**, *56*, 8007.
[18] S. Suckert, M. Rams, L. Germann, D. M. Cegiełka, R. E. Dinnebier, C. Näther, *Cryst. Growth Des.* **2017**, *17*, 3997.
[19] S. Suckert, I. Jess, C. Näther, *Z. Anorg. Allg. Chem.* **2017**, *643*, 721.
[20] D. A. Buckingham, *Coord. Chem. Rev.* **1994**, *135*, 587.
[21] C. Bartual-Murgui, L. Piñeiro-López, F. J. Valverde-Muñoz, M. C. Muñoz, M. Seredyuk, J. A. Real, *Inorg. Chem.* **2017**, *56*, 13535.
[22] J. Werner, M. Rams, Z. Tomkowicz, T. Runčevski, R. E. Dinnebier, S. Suckert, C. Näther, *Inorg. Chem.* **2015**, *54*, 2893.
[23] J. Werner, T. Runčevski, R. Dinnebier, S. G. Ebbinghaus, S. Suckert, C. Näther, *Eur. J. Inorg. Chem.* **2015**, 3236.
[24] T. Neumann, M. Ceglarska, M. Rams, L. S. Germann, R. E. Dinnebier, S. Suckert, I. Jess, C. Näther, *Inorg. Chem.* **2018**, *57*, 3305.
[25] C. D. Mekuimemba, F. Conan, A. J. Mota, M. A. Palacios, E. Colacio, S. Triki, *Inorg. Chem.* **2018**, *57*, 2184.
[26] A. R. Nassief, M. Abdel-Hafiez, A. Hassen, A. S. G. Khalil, M. R. Saber, *J. Magn. Magn. Mater.* **2018**, *452*, 488.
[27] A. Das, K. Bhattacharya, S. Giri, A. Ghosh, *Polyhedron* **2017**, *134*, 295.
[28] J. L. Guillet, I. Bhowmick, M. P. Shores, C. J. A. Daley, M. Gembicky, J. A. Golen, A. L. Rheingold, L. H. Doerrer, *Inorg. Chem.* **2016**, *55*, 8099.
[29] E. Shurdha, C. E. Moore, A. L. Rheingold, S. H. Lapidus, P. W. Stephens, A. M. Arif, J. S. Miller, *Inorg. Chem.* **2013**, *52*, 10583.
[30] E. Shurdha, S. H. Lapidus, P. W. Stephens, C. E. Moore, A. L. Rheingold, J. S. Miller, *Inorg. Chem.* **2012**, *51*, 9655.
[31] R. González, A. Acosta, R. Chiozzone, C. Kremer, D. Armentano, G. De Munno, M. Julve, F. Lloret, J. Faus, *Inorg. Chem.* **2012**, *51*, 5737.
[32] J. Palion-Gazda, B. Machura, F. Lloret, M. Julve, *Cryst. Growth Des.* **2015**, *15*, 2380.
[33] C. Wellm, M. Rams, T. Neumann, M. Ceglarska, C. Näther, *Cryst. Growth Des.* **2018**, *18*, 3117.
[34] S. Suckert, M. Rams, M. Böhme, L. S. Germann, R. E. Dinnebier, W. Plass, J. Werner, C. Näther, *Dalton Trans.* **2016**, *45*, 18190.
[35] O. V. Nesterova, S. R. Petrusenko, V. N. Kokozay, B. W. Skelton, J. Jezierska, W. Linert, A. Ozarowski, *Dalton Trans.* **2008**, 1431.
[36] S. Banerjee, M. G. B. Drew, C.-Z. Lu, J. Tercero, C. Diaz, A. Ghosh, *Eur. J. Inorg. Chem.* **2005**, *2005*, 2376.
[37] J. Werner, Z. Tomkowicz, T. Reinert, C. Näther, *Eur. J. Inorg. Chem.* **2015**, 3066.
[38] M. Mousavi, V. Bereau, C. Duhayon, P. Guionneau, J.-P. Sutter, *Chem. Commun.* **2012**, *48*, 10028.
[39] A. Switlicka, K. Czerwinska, B. Machura, M. Penkala, A. Bienko, D. Bienko, W. Zierkiewicz, *CrystEngComm.* **2016**, *18*, 9042.
[40] S. Petrosyants, Z. Dobrokhotova, A. Ilyukhin, N. Efimov, Y. Mikhlina, V. Novotortsev, *Inorg. Chim. Acta* **2015**, *434*, 41.
[41] S. P. Petrosyants, Z. V. Dobrokhotova, A. B. Ilyukhin, N. N. Efimov, A. V. Gavrikov, P. N. Vasilyev, V. M. Novotortsev, *Eur. J. Inorg. Chem.* **2017**, *2017*, 3561.
[42] S. Wöhlert, T. Fic, Z. Tomkowicz, S. G. Ebbinghaus, M. Rams, W. Haase, C. Näther, *Inorg. Chem.* **2013**, *52*, 12947.
[43] S. Wöhlert, Z. Tomkowicz, M. Rams, S. G. Ebbinghaus, L. Fink, M. U. Schmidt, C. Näther, *Inorg. Chem.* **2014**, *53*, 8298.
[44] C. Näther, S. Wöhlert, J. Boeckmann, M. Wriedt, I. Jeß, *Z. Anorg. Allg. Chem.* **2013**, *639*, 2696.
[45] S. Wöhlert, T. Runčevski, R. E. Dinnebier, S. G. Ebbinghaus, C. Näther, *Cryst. Growth Des.* **2014**, *14*, 1902.
[46] S. Wöhlert, U. Ruschewitz, C. Näther, *Cryst. Growth Des.* **2012**, *12*, 2715.
[47] M. Rams, M. Böhme, V. Kataev, Y. Krupskaya, B. Büchner, W. Plass, T. Neumann, Z. Tomkowicz, C. Näther, *Phys. Chem. Chem. Phys.* **2017**, *19*, 24534.
[48] M. Rams, Z. Tomkowicz, M. Böhme, W. Plass, S. Suckert, J. Werner, I. Jess, C. Näther, *Phys. Chem. Chem. Phys.* **2017**, *19*, 3232.
[49] K. Müller-Buschbaum, *Z. Anorg. Allg. Chem.* **2005**, *631*, 811.
[50] S. L. James, C. J. Adams, C. Bolm, D. Braga, P. Collier, T. Friscic, F. Grepioni, K. D. M. Harris, G. Hyett, W. Jones, A. Krebs,

J. Mack, L. Maini, A. G. Orpen, I. P. Parkin, W. C. Shearouse, J. W. Steed, D. C. Waddell, *Chem. Soc. Rev.* **2012**, *41*, 413.
[51] D. Braga, S. L. Giaffreda, F. Grepioni, A. Pettersen, L. Maini, M. Curzi, M. Polito, *Dalton Trans.* **2006**, 1249.
[52] C. J. Adams, P. C. Crawford, A. G. Orpen, T. J. Podesta, B. Salt, *Chem. Comm.* **2005**, 2457.
[53] S. Suckert, S. Wöhlert, C. Näther, *Z. Naturforsch.* **2016**, *71b*, 381.
[54] S. Suckert, H. Terraschke, H. Reinsch, C. Näther, *Inorg. Chim. Acta* **2017**, *461*, 290.
[55] S. Wöhlert, T. Runčevski, R. E. Dinnebier, C. Näther, *Z. Anorg. Allg. Chem.* **2013**, *639*, 2648.
[56] P. Lumme, I. Mutikainen, E. Lindell, *Inorg. Chim. Acta* **1983**, *71*, 217.
[57] P. M. Takahashi, L. P. Melo, R. C. G. Frem, A. V. G. Netto, A. E. Mauro, R. H. A. Santos, J. G. Ferreira, *J. Mol. Struct.* **2006**, *783*, 161.
[58] H. Yan, *Acta Crystallogr.* **2007**, *E63*, m2602.
[59] P. B. da Silva, R. C. G. Frem, A. V. G. Netto, A. E. Mauro, J. G. Ferreira, R. H. A. Santos, *Inorg. Chem. Commun.* **2006**, *9*, 235.
[60] K. Robinson, G. V. Gibbs, P. H. Ribbe, *Science* **1971**, *172*, 567.
[61] K. Al-Farhan, B. Beagley, O. El-Sayrafi, G. A. Gott, C. A. McAuliffe, P. P. M. Rory, R. G. Pritchard, *J. Chem. Soc. Dalton Trans.* **1990**, 1243.
[62] Y. Jin, Y.-X. Che, J.-M. Zheng, *J. Coord. Chem.* **2007**, *60*, 2067.
[63] G. M. Sheldrick, *Acta Crystallogr.* **2008**, *A64*, 112.
[64] G. M. Sheldrick, *Acta Crystallogr.* **2015**, *C71*, 3.
[65] X-Red (version 1.11), Program for Data Reduction and Absorption Correction, STOE & Cie GmbH, Darmstadt (Germany) **1998**.
[66] X-Shape (version 1.03), Program for the Crystal Optimization for Numerical Absorption Correction, STOE & Cie GmbH, Darmstadt (Germany) **1998**.
[67] X-Area (version 1.44), Program Package for Single Crystal Measurements, STOE & Cie GmbH, Darmstadt (Germany) **2008**.

Graphical synopsis

Aleksej Jochim and Christian Näther

Formation of di- and polynuclear Mn(II) thiocyanate pyrazole complexes in solution and in the solid state

https://doi.org/10.1515/znb-2018-0104
Z. Naturforsch. 2018; x(x)b: xxx–xxx